

# High precision determination of the $Q^2$ -evolution of the Bjorken Sum

A. Deur<sup>1</sup>, Y. Prok<sup>2,1</sup>, V. Burkert<sup>1</sup>, D. Crabb<sup>3</sup>, F.-X. Girod<sup>1</sup>,  
 K. A. Griffioen<sup>4</sup>, N. Guler<sup>2\*</sup>, S. E. Kuhn<sup>2</sup> and N. Kvaltine<sup>3</sup>  
<sup>1</sup>Thomas Jefferson National Accelerator Facility, Newport News, VA 23606  
<sup>2</sup>Old Dominion University, Norfolk, VA 23529  
<sup>3</sup>University of Virginia, Charlottesville, VA 22904  
<sup>4</sup>College of William and Mary, Williamsburg, VA 23187

(Dated: December 3, 2024)

We present a significantly improved determination of the Bjorken Sum for  $0.6 \leq Q^2 \leq 4.8$  GeV<sup>2</sup> using precise new  $g_1^p$  and  $g_1^n$  data taken with the CLAS detector at Jefferson Lab. A higher-twist analysis of the  $Q^2$ -dependence of the Bjorken Sum yields the twist-4 coefficient  $f_2^{p-n} = -0.064 \pm 0.009 \pm_{0.036}^{0.032}$ . This leads to the color polarizabilities  $\chi_E^{p-n} = -0.032 \pm 0.024$  and  $\chi_B^{p-n} = 0.032 \pm 0.013$ . The strong force coupling is determined to be  $\alpha_s^{\overline{\text{MS}}}(M_Z^2) = 0.1226 \pm 0.0068$ , which has an uncertainty a factor of 1.5 smaller than earlier estimates using polarized DIS data. This improvement makes the comparison between  $\alpha_s$  extracted from polarized DIS and other techniques a valuable test of QCD.

PACS numbers: 13.60.-r, 11.55.Hx, 25.30.Rw

## INTRODUCTION

The Bjorken Sum Rule [1] is a cornerstone in the study of nucleon spin structure. It has been investigated via polarized deep inelastic scattering (DIS) at SLAC, CERN, DESY [2]-[8] and Jefferson Lab (JLab) [9]-[12]. In the limit of infinite squared four-momentum transfer  $Q^2$  the sum rule is [1]:

$$\Gamma_1^{p-n} \equiv \Gamma_1^p - \Gamma_1^n \equiv \int_0^1 dx (g_1^p(x) - g_1^n(x)) = \frac{g_A}{6}, \quad (1)$$

where  $g_1^p$  and  $g_1^n$  are the spin-dependent proton and neutron structure functions, respectively,  $g_A$  is the nucleon flavor-singlet axial charge, and  $x$  is the Bjorken scaling variable. At a finite  $Q^2$  large enough so that partonic degrees of freedom are relevant, the Bjorken Sum Rule has been generalized to account for perturbative QCD (pQCD) radiative corrections (the leading-twist term) and non-perturbative power corrections (higher-twist terms). In the  $\overline{\text{MS}}$  scheme, the sum rule becomes [13]:

$$\Gamma_1^{p-n} = \frac{g_A}{6} \left[ 1 - \frac{\alpha_s}{\pi} - 3.58 \left( \frac{\alpha_s}{\pi} \right)^2 - 20.21 \left( \frac{\alpha_s}{\pi} \right)^3 + \dots \right] + (2) \sum_{i=2,3,\dots}^{\infty} \frac{\mu_{2i}^{p-n}(Q^2)}{Q^{2i-2}},$$

where the strong coupling  $\alpha_s$  has itself the form of a perturbative series depending on  $Q^2$ , and the  $Q^2$ -dependence of the higher-twist coefficients  $\mu_{2i}^{p-n}(Q^2)$  is calculable

from pQCD. The logarithmic  $Q^2$ -dependence induced by the pQCD radiative corrections that dominate for  $\alpha_s \ll 1$  has allowed QCD to be established as the correct theory of the strong force. In turn, the higher-twist power corrections  $\mu_{2i}/Q^{2i-2}$  characterize QCD in a stronger coupled regime with typically  $\alpha_s > 0.3$ . Here, at lower  $Q^2$ , partons start to interact strongly and react more and more coherently to the probing particles. Thus, the higher-twists describe the transition between the partonic and hadronic degrees of freedom for the strong force.

The isovector nature of the Bjorken integral makes it a simpler quantity to understand theoretically than the integrals for the proton or neutron separately. This is particularly useful for nucleon structure calculations performed in different  $Q^2$  ranges that reflect large or small  $\alpha_s$ . These regimes, with their suitable calculation techniques, are summarized below.

- For  $Q^2$  above a few GeV<sup>2</sup>, the partonic degrees of freedom are relevant. Here, pQCD can be tested through the leading-twist part of Eq. (2). The subtraction of  $\Gamma_1^n$  from  $\Gamma_1^p$  removes the nucleon matrix elements  $a_0$  and  $a_8$ , and provides a rigorous QCD prediction. The subtraction also cancels the gluon and quark-singlet contributions to the  $Q^2$ -dependence of the sum rule.
- At intermediate  $Q^2$  (from a few GeV<sup>2</sup> down to a few tenths of GeV<sup>2</sup>), non-perturbative contributions affect the  $Q^2$ -dependence. Lattice QCD is the leading calculational technique in this regime. The isovector nature of  $\Gamma_1^{p-n}$  simplifies lattice calculations by removing all disconnected diagrams, which are CPU-expensive to compute [14].
- At low  $Q^2$  (below a few tenths of a GeV<sup>2</sup>), chiral perturbation theory, which uses effective hadronic,

\*Present address: Los Alamos National Laboratory, Los Alamos, New Mexico 87544

rather than fundamental partonic, degrees of freedom, is applicable. The suppression of the  $\Delta_{1232}$  resonance contribution to  $\Gamma_1^{p-n}$  facilitates the chiral perturbation theory calculations, making these predictions more robust [15].

New data from the JLab CLAS EG1-DVCS experiment, taken on polarized proton and deuteron targets, have become available [16]. The kinematics of new data largely overlap the higher  $Q^2$  coverage of earlier JLab data [9], [11], but with smaller statistical errors. On the other hand, the previous JLab polarized data set covers lower  $Q^2$  and higher  $x$ . Put together with these data, the EG1-DVCS data allow us to study the Bjorken Sum at higher  $Q^2$  and with improved statistical precision. Studies of the earlier data showed the necessity of precise measurements at moderately large  $Q^2$ , greater than  $\simeq 2 \text{ GeV}^2$ , in order to extract higher-twists, because of the small magnitude of their total contribution. As Eq. (2) suggests, it may seem to be beneficial to determine higher-twists at lower  $Q^2$  where the unmeasured low- $x$  contribution to  $\Gamma_1^{p-n}$  is smaller, the data are more precise, and the higher-twists are enhanced. However, in the standard perturbative approach, this may not be reliable due to the following effects:

- Higher-order twist effects at low  $Q^2$  rise quickly and the short  $Q^2$ -range over which this rise occurs is too small to disentangle these higher-twists.
- There is an increasing uncertainty on the twist-2 part because the proximity of the Landau pole magnifies the uncertainty on  $\alpha_s$ .
- While higher orders leading-twist terms are necessary at low  $Q^2$ , the renormalon problem [17] jeopardizes the convergence of the series and increase the uncertainties due to truncations.

It is possible to avoid part of the difficulty by developing expressions for the Bjorken Sum Rule with better convergence properties, as explored in [18]. We will not pursue this interesting path, and will instead remain consistent with the previous analyses [9], [11] and [19], using the standard expansion, Eq. (2), since the higher  $Q^2$  kinematics of EG1-DVCS are suited to this approach.

## ANALYSIS

### Bjorken Sum

The extraction of  $g_1^p$  and  $g_1^d$  from the EG1-DVCS data is described in Ref. [16]. The  $Q^2$ -coverage and the integration limits are given in Table 1. Since moments must be integrated over all  $x$ , a model must supplement the data at low- $x$ . We describe the model in the next section. The  $Q^2$  values for  $\Gamma_1^p$  and  $\Gamma_1^d$  often differ slightly.

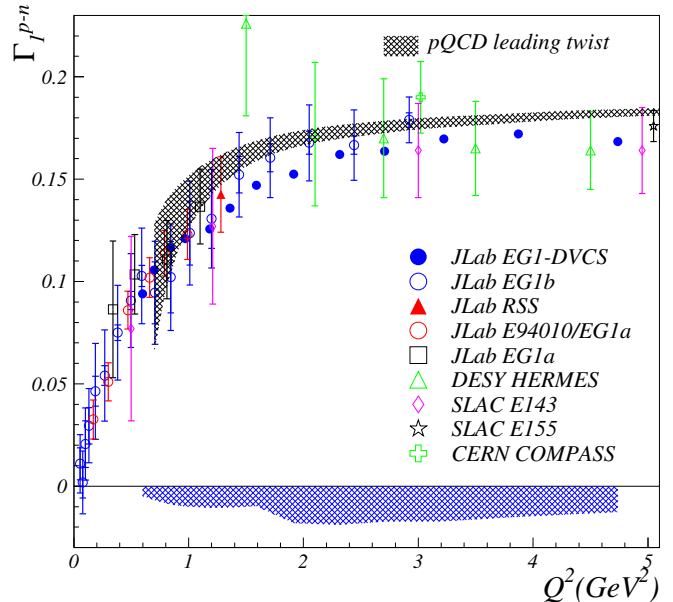


FIG. 1: (Color online.) The Bjorken Sum  $\Gamma_1^{p-n}$ . The solid blue circles give our results. The blue band is the systematic uncertainty. Other symbols show the world data. For those, the inner error bar indicates the statistical uncertainty and the outer error bar the quadratic sum of the statistic and systematic uncertainties. The gray band represents the leading-twist NNLO pQCD calculation in the  $\overline{\text{MS}}$  scheme.

When combining them into  $\Gamma_1^{p-n}$ , the  $Q^2$  was chosen as the mean between the proton and deuteron  $Q^2$  values, weighted by the statistical uncertainties on  $\Gamma_1^p$  and  $\Gamma_1^d$ . Both  $\Gamma_1^p$  and  $\Gamma_1^d$  were linearly interpolated to the common  $Q^2$  before being combined into the Bjorken Sum,  $\Gamma_1^{p-n} = 2\Gamma_1^p - \Gamma_1^d / (1 - 1.5\omega_d)$ , with  $\omega_d = 0.05 \pm 0.01$  [20] (Here,  $\Gamma_1^d$  is calculated as “per nucleus”, not as “per nucleon”). The result for  $\Gamma_1^{p-n}$  is plotted in Fig. 1 together with data from the previous experiments conducted at SLAC [3], [5], DESY [7], JLab [9]-[11], and CERN [8]. The elastic contribution ( $x=1$ ) is not included. Overall, the  $Q^2$ -behavior of  $\Gamma_1^{p-n}$  is smooth within systematic uncertainties. There is good agreement between the world data on  $\Gamma_1^{p-n}$  and EG1-DVCS, including cases where the neutron moment,  $\Gamma_1^n$ , is obtained from a  $^3\text{He}$  target [4], [7], [9]. We also plot the leading-twist NNLO pQCD calculation based on Eq. (2) (gray band). The width of the band stems from the uncertainty in the strong coupling  $\alpha_s$ .

In order to evaluate the unmeasured parts of  $\Gamma_1^p$  and  $\Gamma_1^n$  at low- $x$ , we need a model for  $g_1^p$  and  $g_2^n$  covering a wide kinematic range. The model that we use here is built upon fits to the world data of the asymmetries  $A_1$  and  $A_2$ , and the unpolarized structure functions  $F_1$  and  $R$ . Those were modeled using a parameterization

$Q^2$ (GeV <sup>2</sup> )	$x$ -range (p)	$x$ -range (d)	$\Gamma_{1,meas}^{p-n}$	$\Gamma_{1,meas+hi.x}^{p-n}$	$\sigma_{meas}^{syst}$	$\sigma_{hi.x}^{syst}$	$\Gamma_{1,tot}^{p-n}$	$\sigma^{syst}$	$\sigma^{stat}$	$\Gamma_{1,meas+hi.x}^{p-n} / \Gamma_{1,tot}^{p-n}$
0.600	0.0695-0.072	0.070-0.074	-0.0001	0.0612	0.0001	0.0029	0.0940	0.0048	0.0005	0.651
0.698	0.0795-0.091	0.081-0.094	0.0031	0.0670	0.0002	0.0054	0.1056	0.0068	0.0005	0.634
0.840	0.0970-0.119	0.099-0.123	0.0079	0.0707	0.0004	0.0079	0.1164	0.0089	0.0006	0.607
0.972	0.110-0.155	0.113-0.168	0.0110	0.0674	0.0008	0.0088	0.1210	0.0099	0.0007	0.557
1.184	0.136-0.210	0.139-0.228	0.0169	0.0628	0.0016	0.0093	0.1257	0.0105	0.0007	0.500
1.361	0.151-0.304	0.168-0.322	0.0414	0.0606	0.0036	0.0082	0.1358	0.0103	0.0009	0.446
1.590	0.179-0.494	0.189-0.494	0.0580	0.0642	0.0083	0.0006	0.1470	0.0098	0.0011	0.437
1.915	0.213-0.804	0.233-0.733	0.0552	0.0542	0.0171	0.0007	0.1524	0.0181	0.0011	0.356
2.316	0.263-0.864	0.271-0.798	0.0523	0.0515	0.0177	0.0001	0.1621	0.0188	0.0008	0.317
2.707	0.304-0.825	0.326-0.769	0.0398	0.0388	0.0157	0.0008	0.1636	0.0173	0.0006	0.237
3.223	0.362-0.901	0.385-0.799	0.0322	0.0311	0.0152	0.0000	0.1697	0.0171	0.0005	0.183
3.871	0.438-0.893	0.463-0.762	0.0227	0.0206	0.0121	0.0002	0.1721	0.0150	0.0004	0.120
4.739	0.531-0.909	0.663-0.738	0.0145	0.0113	0.0081	0.0002	0.1684	0.0126	0.0002	0.067

TABLE I: Kinematic ranges and partial and full Bjorken Sums. Columns 2 and 3 give the  $x$ -ranges over which the proton and deuteron data are measured, respectively. Column 4 provides the partial sum  $\Gamma_{1,meas}^{p-n}$  from EG1-DVCS. Column 5 gives the measured sum supplemented by a fit to earlier JLab data in the high- $x$  domain,  $\Gamma_{1,meas+hi.x}^{p-n}$ . The experimental systematic uncertainty is denoted by  $\sigma_{meas}^{syst}$ . The high- $x$  interpolation is  $\sigma_{hi.x}^{syst}$ . Column 8 gives the total  $\Gamma_{1,tot}^{p-n}$  sum, and  $\sigma^{syst}$  and  $\sigma^{stat}$  are the total (experimental, high- $x$  and low- $x$ ) systematics and statistical uncertainties on  $\Gamma_{1,tot}^{p-n}$ , respectively. The ratio of the sum without the low- $x$  estimate,  $\Gamma_{1,meas+hi.x}^{p-n}$ , over the total is given by  $\Gamma_{1,meas+hi.x}^{p-n} / \Gamma_{1,tot}^{p-n}$ .

of the world data that fits both the DIS and resonance regions with an average precision of 2 to 3% [21]. The systematic uncertainty was calculated by varying either  $F_1$  or  $R$  by the average uncertainty of the fit (2-3%) and recalculating all quantities of interest.

For  $A_1$  and  $A_2$  we used our own phenomenological fit to the world data, including all DIS results from SLAC, HERA, CERN and Jefferson Lab and data in the resonance region from MIT Bates [22] and Jefferson Lab. The asymmetry  $A_2$  in the DIS region was modeled using the Wandzura-Wilczek relation [23]. For systematic variations, we included a simple functional form for an additional twist-3 term introduced by E155 [5], and a model constrained by the Soffer Bound [24].

At very low values of  $x$ , uncertainties in the model increase rapidly, so we imposed a lower limit at  $x = 0.001$ . Below this value, we extrapolate directly the isovector part of the structure function  $g_1$  using the Regge parameterization  $g_1^{p-n}(x) = g_1^{p-n}(x_0)(x_0/x)^{0.89}$ . We chose the power 0.89 so that the Bjorken Sum at  $Q^2 = 5$  GeV<sup>2</sup> from the world data satisfies the Bjorken Sum Rule. Such a parameterization agrees within 50% with the low- $x$  parameterization determined in Ref. [25]. We assumed a 100% uncertainty on this contribution. The part below  $x = 0.001$  contributes up to about 5% of the total sum.

EG1-DVCS does not cover the higher- $x$  values. There, we used a fit to earlier JLab data [9], [11].

The new determination of  $\Gamma_1^{p-n}$  is shown together with phenomenological models in Fig. 2. The Burkert-Ioffe model (black line) is an extrapolation of DIS data based on vector meson dominance, complemented by a parameterization of the resonance contribution [26]. The Soffer-Teryaev model (red line) uses the smoothness of  $g_1 + g_2$

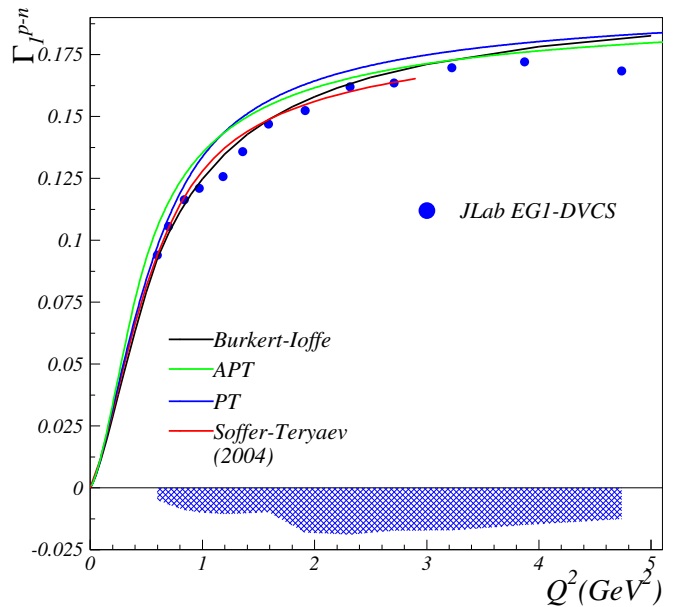


FIG. 2: (Color online.) The Bjorken Sum  $\Gamma_1^{p-n}$  from EG1-DVCS (solid blue circles) compared with the phenomenological models described in the main text.

with  $Q^2$  to extrapolate DIS data to lower  $Q^2$  [27]. The two other lines are from Ref. [28]. They are updates of the Soffer-Teryaev model using standard perturbation theory (PT, blue line) and ghost-free analytical perturbation theory (APT, green line) which now includes the higher-twist terms  $\mu_4$  and  $\mu_6$ . The higher-twist values

were obtained from fits to the JLab data [18]. The APT formalism aims at reducing the influence of the Landau pole divergence at  $\Lambda_{QCD}$ .

The precision of the new determination of  $\Gamma_1^{p-n}$  allows us for the first time to see that the data lie systematically below the leading-twist NNLO pQCD prediction shown by the hatched band in Fig. 1. Although a large point-to-point correlated contribution to the systematic uncertainty could still make the data compatible with the leading-twist calculation, this difference and the steeper  $Q^2$ -evolution of the data compared to the leading-twist calculation for  $Q^2 > 1.5 \text{ GeV}^2$  suggest a negative higher-twist contribution to  $\Gamma_1^{p-n}$ . These features are quantitatively analyzed in the next section.

### Higher-twist analysis

In this section, we determine quantitatively the higher-twist contributions to  $\Gamma_1^{p-n}$ . In addition to the EG1-DVCS data, we use all other world data, including the  $Q^2 = 10 \text{ GeV}^2$  SMC data [6] not visible in Fig. 1.

The moment  $\Gamma_1^{p-n}$  can be expanded in powers of  $1/Q^2$ , see Eq. (2). The coefficient of the first power correction is [29]:

$$\mu_4^{p-n} = \frac{M^2}{9} (a_2^{p-n} + 4d_2^{p-n} + 4f_2^{p-n}), \quad (3)$$

where  $M$  is the nucleon mass. The coefficient  $a_2^{p-n}$  is the twist-2 target mass correction expressed as

$$a_2^{p-n} = \int_0^1 dx (x^2 g_{1,LT}^{p-n}), \quad (4)$$

in which  $g_{1,LT}^{p-n}$  is the leading-twist part of  $g_1^{p-n}$ . The twist-3 matrix element  $d_2^{p-n}$  is given by

$$d_2^{p-n} = \int_0^1 dx x^2 (2g_1^{p-n} + 3g_2^{p-n}), \quad (5)$$

and  $f_2^{p-n}$  is the twist-4 contribution to be extracted. These coefficients depend logarithmically on  $Q^2$  but apart for  $f_2^{p-n}$ , we will neglect this small dependence in our analysis and use their values at  $Q^2 = 1 \text{ GeV}^2$ . The LO pQCD dependence of  $f_2^{p-n}$  is accounted for using its anomalous dimension [29]. The coefficient  $a_2$  is a kinematical higher-twist [30] containing no additional information than is provided by the leading twist parton distributions. The dynamical higher-twist  $d_2$  can be measured directly from polarized lepton scattering off transversely and longitudinally polarized targets. We are interested here in the dynamical higher-twist  $f_2$  which can be obtained only from studying the  $Q^2$ -evolution of the moment of  $g_1$ .

For a consistent higher-twist analysis, the elastic contribution to  $\Gamma_1^{p-n}$  must be added [31] because it contains large higher-twist terms, as witnessed by the fast decrease of the elastic form factors with  $Q^2$ . At  $Q^2 \sim 1 \text{ GeV}^2$ , the elastic contribution remains sizable and cannot be neglected. To determine it, we used the elastic form factor fits from Ref. [32] for the proton and Ref. [33] for the neutron. The strong coupling  $\alpha_s$  enters in Eq. (2). We computed it in the  $\overline{\text{MS}}$  scheme to next-to-leading order ( $\beta_1$ ) in the  $\alpha_s$ 's  $\beta$ -series. A fit of polarized parton distributions [34] was used to determine  $a_2^{p-n}$ . At  $Q^2 = 1 \text{ GeV}^2$ ,  $a_2^{p-n} = 0.031 \pm 0.010$ . The proton twist-3  $d_2^p$  matrix element is obtained from [10]. Data from Refs. [35], [10], [19], [36], [37] and lattice calculations [38] suggest that for the neutron,  $d_2^n$  is negligible at  $Q^2 > 2 \text{ GeV}^2$ . We use  $d_2^n = 0.000 \pm 0.001$  at  $Q^2 = 5 \text{ GeV}^2$ . Evolving  $d_2^{n-p}$  from  $Q^2 = 5 \text{ GeV}^2$  to  $1 \text{ GeV}^2$  using the anomalous dimension calculated in [29], we obtain  $d_2^{p-n} = 0.008 \pm 0.0036$ .

The world data on  $\Gamma_1^{p-n}$ , including those in Table I, except for the  $Q^2 = 4.7 \text{ GeV}^2$  point for which the estimated low- $x$  contribution to the integral is large, were fit to extract  $f_2^{p-n}$  using Eqs. (2) and (3) with  $\alpha_s$ ,  $a_2^{p-n}$  and  $d_2^{p-n}$  determined as discussed above. To account for twist-6 and greater, we add a coefficient  $\mu_6^{*p-n}/Q^4$  to the fit. The asterisk reminds us that this coefficient includes not only the true  $\mu_6^{p-n}/Q^4$  correction, but also compensations for higher order terms  $\mu_N^{p-n}$  with  $N > 6$ . That is,  $\mu_6^* = \mu_6 + \sum_{i=2,4,\dots} \mu_{i+6}/Q^i$ . The equation shows explicitly that  $\mu_6^*$  depends on  $Q^2$  (beside its logarithmic dependence that we neglect). Approximating  $\mu_6^*$  to be  $Q^2$ -independent is justified if the power series converges, and this should affect  $f_2$  minimally but may lead to a  $\mu_6^*$  significantly different from the actual  $\mu_6$ . We have two completely free parameters,  $f_2$  and  $\mu_6^*$ , in the fit, plus a third parameter, the axial charge  $g_a$ , which is bounded by its experimental uncertainty range ( $g_a = 1.27 \pm 0.04$ ).

As published, the world data on  $\Gamma_1^{p-n}$  are corrected for the missing low- $x$  contribution using various estimates, depending on the publication. For the consistency of this analysis, the low- $x$  estimates of the world data were recalculated using the model discussed in the Bjorken Sum section. For all JLab data sets (Refs. [9], [11] and the present data), the point-to-point uncorrelated uncertainties have been separated from the correlated ones using the *unbiased estimate*, and added in quadrature to the statistical uncertainties. The correlated systematics were propagated independently into the fit result, as was the uncertainty arising from  $\alpha_s$ . The uncertainties stemming from  $a_2^{p-n}$  and  $d_2^{p-n}$  are negligible. Table II gives the best fits for several  $Q^2$  ranges, since there is no prescription as to where in  $Q^2$  the fit should start. The results are consistent. The first uncertainty listed is the quadratic sum of the statistical and point-to-point uncorrelated uncertainties. The second is the point-to-point correlated uncertainty. We do not report the parameter  $g_A$  in Table II. Its fit value is always  $g_a = 1.305$ , which corre-

sponds to the upper bound of its variation range. This is due to the positive elastic contribution that dominates the  $Q^2$ -dependence of the sum for  $Q^2 \lesssim 1 \text{ GeV}^2$ . For  $Q^2 \lesssim 1 \text{ GeV}^2$ , the  $Q^2$ -dependence of the elastic contribution is less steep than that of the  $1/Q^4$  or  $1/Q^6$  higher-twist terms. These too-steep behaviors are compensated in the fits in part by a negative  $f_2^{p-n}$  and in part by an increased leading-twist contribution, i.e by a larger  $g_A$ . This compensates for the too-steep  $Q^2$ -behavior of  $\mu_6$  or  $\mu_8$  compared to the data, since both the leading-twist and the  $f_2$  contributions have slopes of opposite signs (their values increase with  $Q^2$ ) to that of  $\mu_6$  or  $\mu_8$  (their values decrease with  $Q^2$ ).

To assess the convergence of the twist series in Eq. (2), we give in Table III the best fits when an additional  $\mu_8^{*p-n}/Q^6$  coefficient is used (the asterisk has the same meaning as for  $\mu_6^*$ ). In these 4-parameter fits,  $\mu_6$  now gives more properly the  $1/Q^4$  power correction). Similar convergence studies were done in [9] and [11], and results for  $\mu_8^{*p-n}$  were consistent with zero with large uncertainties ranging from 0.04 to 0.09 depending on the  $Q^2$  at which the fit starts. Now, the precision of the data allows us to determine the magnitude and sign of  $\mu_8^{*p-n}$ . The question of the convergence of the higher-twist series arises naturally, since Refs. [9] and [11] indicated that  $\mu_4^{p-n}$  and  $\mu_6^{*p-n}$  are of similar magnitudes but opposite signs at  $Q^2 \simeq 1 \text{ GeV}^2$ . This suggested a poor convergence of the twist series, at least in the  $Q^2$  ranges concerned. With better data, it now appears that  $\mu_8^{*p-n}$  and  $\mu_4^{p-n}$  are of similar size while  $\mu_6^{p-n}$  is small. This indicates that Eq. (2) converges only for  $Q^2 \gtrsim 1 \text{ GeV}^2$ . The central value of  $\mu_6^{p-n}$  is significantly smaller than that of  $\mu_6^{*p-n}$ , once  $\mu_8^{*p-n}$  is accounted for. However,  $\mu_6^{p-n}$  and  $\mu_6^{*p-n}$  are still compatible within uncertainties. A systematic study done with the models [26] and [27] is described in Ref. [39]. It was performed to better understand the convergence of the twist series given a truncation at  $\mu_{max}^*$  (corresponding to  $\mu_6^*$  for the 3 parameter fit and to  $\mu_8^*$  for the 4 parameter fit) and a choice of  $Q_{min}^2$ , the lowest  $Q^2$  used in the fit. The conclusion from the present experimental higher-twist extraction agrees with the model-based conclusions of Ref. [39]:

- The extraction of  $f_2^{p-n}$  is stable as  $Q_{min}^2$  and  $\mu_{max}$  are modified in the ranges  $0.6 \leq Q_{min}^2 \leq 3 \text{ GeV}^2$  and  $\mu_6^{p-n} \leq \mu_{max}^{p-n} \leq \mu_{12}^{p-n}$  for the model study, and in the range  $0.6 \leq Q_{min}^2 \leq 1 \text{ GeV}^2$  and with  $\mu_{max}^{p-n} = \mu_6^{p-n}$  or  $\mu_8^{p-n}$  for the present experimental study.
- The coefficient  $\mu_6^{p-n}$  is small, typically a factor of 6 smaller than  $f_2^{p-n}$  for the model and a factor of 3 smaller for the data, although a 3-parameter fit gives a larger  $\mu_6^{p-n}$  of similar magnitude to  $f_2^{p-n}$ . Increasing the number of parameters decreases  $\mu_6^{p-n}$ . This implies the convergence of the series for  $Q^2 \gtrsim 1 \text{ GeV}^2$ .

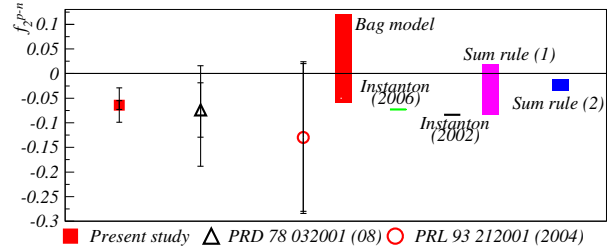


FIG. 3: Three-parameter fit result for  $f_2^{p-n}$  from the present study (square) and Refs. [11] (triangle) and [9] (circle). The inner error bar represents the point-to-point uncorrelated uncertainty and the outer error bar is the quadratic sum of the point-to-point correlated and uncorrelated uncertainties. Theoretical calculations [41]-[44] are shown on the right.

- At  $Q^2 \simeq 1 \text{ GeV}^2$ , there is an approximate cancellation of the higher-twist terms (independent of  $Q_{min}^2$ ).

The overall uncertainty on  $f_2^{p-n}$  is dominated by the unmeasured low- $x$  region. The uncertainty from  $\alpha_s$  becomes important only for fits starting at the lowest  $Q_{min}^2$  ( $0.66 \text{ GeV}^2$ ) since the effect of the Landau pole becomes important as  $Q$  gets close to  $\Lambda_{QCD}$ . The JLab data were all taken with beam energies of up to about 6 GeV. The upcoming 12 GeV program at Jefferson Lab will significantly reduce this dominant uncertainty since the measured fraction of  $\Gamma_1^{p-n}$  above  $Q^2 = 2.5 \text{ GeV}^2$  will at least double compared to the present measurement [40].

The twist-4 coefficient  $f_2^{p-n}$  obtained from the 3-parameter fit over the  $0.84$ - $10 \text{ GeV}^2$   $Q^2$  range is plotted in Fig. 3 along with the results of Refs. [11] and [9] obtained using the same fit range, and theoretical predictions [41]-[44]. The magnitude and sign of  $f_2^{p-n}$  agree with the analysis performed on  $g_1(x)$  in Ref. [45], which found that twist-4 corrections to  $g_1(x)$  are sizeable but change sign at  $x \sim 0.4$  for the proton, leading to a small integrated value. Our result expressed as  $\mu_4^{p-n}/M^2 = -0.021 \pm 0.016$  (3-parameter fit with the  $0.84$ - $10 \text{ GeV}^2$   $Q^2$  range) also agrees with the several extractions done in Ref. [18], which are typically around  $\mu_4^{p-n}/M^2 \sim -0.05$  with a spread of 0.02.

### Color electric and magnetic polarizabilities

The twist-3 and 4 terms of the  $\mu_4$  coefficient, Eq. (3), yield the color electric and magnetic polarizabilities [41], [46],  $\chi_E = \frac{2}{3}(2d_2 + f_2)$  and  $\chi_B = \frac{1}{3}(4d_2 - f_2)$  respectively. Using the value of  $f_2^{p-n}$  from the 3-parameter fit starting at  $Q_{min}^2 = 0.84 \text{ GeV}^2$  and  $d_2^{p-n} = 0.0080 \pm 0.0036$ , we obtain  $\chi_E^{p-n} = -0.032 \pm 0.024$  and  $\chi_B^{p-n} = 0.032 \pm 0.013$ . The point-to-point correlated and uncorrelated uncertainties on  $f_2^{p-n}$  were symmetrized and added

$Q^2$ range	$f_2^{p-n}$	$\mu_6^{*p-n}$ (GeV <sup>4</sup> )	$\chi^2/\text{d.o.f}$
0.66-10.0 GeV <sup>2</sup>	$-0.093 \pm 0.006 \pm_{0.037}^{0.026}$	$0.087 \pm 0.002 \pm_{0.022}^{0.033}$	1.03
0.84-10.0 GeV <sup>2</sup>	$-0.064 \pm 0.009 \pm_{0.036}^{0.032}$	$0.070 \pm 0.004 \pm_{0.018}^{0.023}$	0.71
1.00-10.0 GeV <sup>2</sup>	$-0.057 \pm 0.010 \pm_{0.043}^{0.039}$	$0.065 \pm 0.005 \pm_{0.019}^{0.021}$	0.72

TABLE II: Values of  $f_2^{p-n}$  and  $\mu_6^{*p-n}$  at  $Q^2=1$  GeV<sup>2</sup> from the 3-parameter fit (the parameter  $g_a$  is not reported in this table, see main text). The two uncertainties given for  $f_2^{p-n}$  and  $\mu_6^{*p-n}$  are the point-to-point uncorrelated (first number) and point-to-point correlated uncertainties (second numbers). The last column gives the  $\chi^2$  per degree of freedom of the fit, with only the point-to-point uncorrelated uncertainties accounted for.

$Q^2$ range	$f_2^{p-n}$	$\mu_6^{p-n}$ (GeV <sup>4</sup> )	$\mu_8^{*p-n}$ (GeV <sup>6</sup> )	$\chi^2/\text{d.o.f}$
0.66-10.0 GeV <sup>2</sup>	$-0.044 \pm 0.010 \pm_{0.054}^{0.055}$	$0.012 \pm 0.010 \pm_{0.034}^{0.024}$	$0.032 \pm 0.006 \pm_{0.017}^{0.023}$	0.63
0.84-10.0 GeV <sup>2</sup>	$-0.035 \pm 0.015 \pm_{0.041}^{0.037}$	$-0.005 \pm 0.020 \pm_{0.009}^{0.008}$	$0.044 \pm 0.014 \pm_{0.010}^{0.019}$	0.66
1.00-10.0 GeV <sup>2</sup>	$-0.020 \pm 0.032 \pm_{0.031}^{0.025}$	$-0.037 \pm 0.032 \pm_{0.019}^{0.019}$	$0.073 \pm 0.022 \pm_{0.013}^{0.018}$	0.67

TABLE III: Same as Table II but for the 4-parameter fit.

in quadrature. The polarizabilities are compatible with those reported in Ref. [11] with a factor of 2 improvement on the uncertainties.

### The strong coupling $\alpha_s$

The strong force coupling at the  $Z^0$  pole,  $\alpha_s(M_Z^2)$ , can be extracted from the Bjorken Sum data by solving Eq. (2) for  $\alpha_s$ , and then evolving  $\alpha_s$  to the  $Z^0$  pole. However, the relative uncertainty for this method is large, typically 30%, and dominated by the model determination of the unmeasured low- $x$  region. Rather than using an absolute measurement, we can obtain  $\alpha_s(M_Z^2)$  more precisely by fitting the  $Q^2$ -dependence of  $\Gamma_1^{p-n}$  [47]. In our case, where we include relatively low  $Q^2$  data points, we must account for  $\mu_4^{p-n}$ . We can neglect the higher orders since  $\mu_6^{p-n}$  is small and  $\mu_8^{*p-n}$  is suppressed as  $1/Q^4$  compared to  $\mu_4^{p-n}$ . Since  $f_2^{p-n}$  was obtained assuming the validity of the Bjorken Sum Rule and using a theoretical  $\alpha_s$ , we must use an independent determination of  $f_2^{p-n}$  to form  $\mu_4^{p-n}$ . We choose  $f_2^{p-n}$  from Ref. [44], for which we assumed a 50% uncertainty. We used a  $\overline{\text{MS}}$  leading-twist expression of  $\Gamma_1^{p-n}$  up to order  $\alpha_s^5$  and estimated the uncertainty due to the truncation of the leading-twist pQCD series by taking the difference between the 4<sup>th</sup> and 5<sup>th</sup> orders. We then evolved the extracted  $\alpha_s$  to the  $Z^0$  mass  $M_Z$  using the evolution equation up to order  $\beta_3$  with  $\Lambda_{QCD}^{\overline{\text{MS}}} = 0.2143 \pm 0.0070$  GeV.

Fitting the values of  $\Gamma_{1,tot}^{p-n}$  in Table I, starting at  $Q_{min}^2 = 2.316$  GeV<sup>2</sup> with  $g_A$  and  $\Lambda_{QCD}$  as fit parameters, we obtain  $\alpha_s^{\overline{\text{MS}}}(M_Z^2) = 0.1226 \pm 0.0068$ . The uncertainty is dominated by the point-to-point uncorrelated uncertainty  $\pm 0.0055$ . The uncertainties from the truncation of the  $\beta$ -series and from  $a_2^{p-n}$ ,  $d_2^{p-n}$  and  $f_2^{p-n}$  are comparatively small. The point-to-point correlated uncertainty is  $\pm 0.0040$ , which is dominated by the low- $x$  estimate. To assess this point-to-point correlated uncertainty, we separated  $\sigma^{syst}$  in Table I into a constant with

respect to  $Q^2$ , which does not contribute to the uncertainty on  $\alpha_s$ , and a  $Q^2$ -dependent part. The latter is estimated by calculating  $\Delta\Gamma = d(\Gamma_{1,tot}^{p-n})/dQ^2 \times (Q^2 \text{ bin size}) \times (\Gamma_{1,tot} - \Gamma_{1,meas})/\Gamma_{1,tot}$  for each  $Q^2$  point. For this expression, the relative amount of the unmeasured low- $x$  contribution,  $(\Gamma_{1,tot} - \Gamma_{1,meas})/\Gamma_{1,tot}$  can be obtained from the last column of Table I. Each  $\Delta\Gamma$  is treated as an additional uncertainty to  $\Gamma_1^{p-n}$  and is added in quadrature to the point-to-point uncorrelated uncertainty.

The Regge exponent determining the (small) contribution to the integral below  $x = 0.001$  was obtained by assuming the validity of the Bjorken Sum Rule at  $Q^2=5$  GeV<sup>2</sup>. This implies evolving Eq. (1) from infinite  $Q^2$  to  $Q^2=5$  GeV<sup>2</sup>. In the process, a value for  $\alpha_s$  must be assumed. However, this initial assumption on  $\alpha_s$  does not bias our determination of  $\alpha_s$ . The contribution from  $x < 0.001$  influences the absolute value of  $\Gamma_1^{p-n}$  at the few percent level. Our  $\alpha_s$  depends on  $x < 0.001$  only *via* the  $Q^2$ -dependence, for which we assigned the conservative uncertainty just discussed.

Our value of  $\alpha_s^{\overline{\text{MS}}}(M_Z^2)$  is compatible with the average world data,  $\alpha_s^{\overline{\text{MS}}}(M_Z^2) = 0.1185 \pm 0.0006$ , and it significantly improves the precision on  $\alpha_s^{\overline{\text{MS}}}(M_Z^2)$  from polarized DIS last reported by the Particle Data Group [48]. The result is less precise than direct measurements at the  $Z^0$  pole, but has similar precision to some of the  $\alpha_s$  results reported by the Particle Data Group. This demonstrates the viability of determining  $\alpha_s$  with polarized DIS data, especially since, as already discussed for  $\Gamma_1^{p-n}$ , the leading uncertainty will be significantly reduced when the 12 GeV JLab data will become available [40] and *a fortiori* if the future polarized EIC becomes available [49].

## SUMMARY

New JLab CLAS data have allowed us to form the Bjorken Sum  $\Gamma_1^{p-n}$  for  $0.60 < Q^2 < 4.74$  GeV<sup>2</sup>. The sum is consistent with previous JLab data and exhibits a char-

acteristically strong  $Q^2$ -behavior in the hadron-parton transition region. The statistical uncertainty is small compared to the systematic uncertainty, which is dominated by the contribution from the unmeasured low- $x$  domain. While the analyses of former JLab data covered the low and intermediate  $Q^2$  regions where hadronic degrees of freedom play a role, the new data cover the intermediate and partonic (high  $Q^2$ ) domains. This is particularly suited for extracting higher-twist coefficients and color polarizabilities. These quantities were extracted from a global analysis of the world data, including the new JLab data presented in this paper. The twist-4 coefficient was confirmed to be relatively large in absolute magnitude:  $f_2^{p-n} = -0.064 \pm 0.036$  compared to the leading-twist coefficient  $\Gamma_1^{p-n,pQCD} = 0.141 \pm 0.013$ , the twist-2 coefficient  $a_2^{p-n} = 0.031 \pm 0.010$ , and the twist-3 coefficient  $d_2^{p-n} = 0.008 \pm 0.003$ . The net higher-twist effect is small around  $Q^2 = 1 \text{ GeV}^2$  because of a cancellation between twist-4 and the sum of higher power corrections that are of opposite sign. Fits with four parameters reveal that the twist-6 contribution is small and the cancellation comes from twist-8 and/or higher contributions. This implies the convergence of the twist series above  $Q^2 \simeq 1 \text{ GeV}^2$ . The color electric and magnetic polarizabilities were extracted with a factor of 2 improvement on the uncertainty compared to earlier analyses. The two polarizabilities are of similar value but opposite sign. From the  $Q^2$ -behavior of  $\Gamma_1^{p-n}$  and a model estimate of  $f_2^{p-n}$ , we extracted  $\alpha_s^{\overline{\text{MS}}}(M_Z^2) = 0.1226 \pm 0.0068$ . The precision is a factor 1.5 better than earlier estimates from polarized DIS, making  $\Gamma_1^{p-n}$  a viable observable for determining  $\alpha_s$ . Its agreement with the other  $\alpha_s$  determined from different observables provides a consistency check of QCD.

We thank J. Soffer and R. S. Pasechnik for providing the curves from [28] and P. Bosted for reading the manuscript and for useful discussions. This work is supported by the U.S. Department of Energy (DOE) and the U.S. National Science Foundation. The Jefferson Science Associates operate the Thomas Jefferson National Accelerator Facility for the DOE under contract DE-AC05-84ER40150, with additional support from DOE grants, DE-FG02-96ER40960 (S. K., N. G., Y. P.) and DE-FG02-96ER41003 (K. G.).

---

[1] J. D. Bjorken, Phys. Rev. **148**, 1467 (1966); Phys. Rev. **D 1**, 465 (1970); Phys. Rev. **D 1**, 1376 (1970).  
[2] P. L. Anthony *et al.*, Phys. Rev. Lett. **71**, 959 (1993); Phys. Rev. **D 54**, 6620 (1996).  
[3] K. Abe *et al.*, Phys. Rev. Lett. **74**, 346 (1995); **75**, 25 (1995); **76**, 587 (1996); Phys. Lett. **B 364**, 61 (1995); Phys. Rev. **D 58**, 112003 (1998).  
[4] K. Abe *et al.*, Phys. Rev. Lett. **79**, 26 (1997); Phys. Lett.

**B 404**, 377 (1997); **B 405**, 180 (1997).  
[5] P. L. Anthony *et al.*, Phys. Lett. **B 458**, 529 (1999); **B 463**, 339 (1999); **B 493**, 19 (2000); **B 553**, 18 (2003).  
[6] D. Adams *et al.*, Phys. Lett. **B 329**, 399 (1994); **B 336**, 125 (1994); **B 357**, 248 (1995); **B 396**, 338 (1997); Phys. Rev. **D 56**, 5330 (1997).  
[7] K. Ackerstaff *et al.*, Phys. Lett. **B 404**, 383 (1997); **B 444**, 531 (1998); A. Airapetian *et al.*, Phys. Lett. **B 442**, 484 (1998); Phys. Rev. Lett. **90**, 092002 (2003). ; A. Airapetian *et al.*, Phys. Rev. **D 75**, 012007 (2007).  
[8] V. Yu. Alexakhin *et al.*, Phys. Lett. **B 647**, 8 (2007); M. G. Alekseev *et al.*, Phys. Lett. **B 690**, 466 (2010).  
[9] A. Deur *et al.*, Phys. Rev. Lett. **93**, 212001 (2004).  
[10] F. R. Wesselmann *et al.*, Phys. Rev. Lett. **98** 132003 (2007); K. Slifer *et al.*, Phys. Rev. Lett. **105** 101601 (2010).  
[11] A. Deur *et al.*, Phys. Rev. **D 78**, 032001, 2008.  
[12] J.-P. Chen, A. Deur, Z.-E. Meziani, Mod. Phys. Lett. **A 20**, 2745 (2005).  
[13] A. L. Kataev, Phys. Rev. **D 50**, 5469 (1994).  
[14] M. Goeckeler *et al.*, Nucl. Phys. Proc. Suppl. **119** 32 (2003).  
[15] V. D. Burkert, Phys. Rev. **D 63**, 097904 (2001).  
[16] Y. Prok *et al.*, (CLAS EG1-DVCS collaboration). In submission (arXiv:1404.6231).  
[17] J. Ellis, E. Gardi, M. Karliner and M. A. Samuel, Phys. Lett. **B 366** 268 (1996).  
[18] K. A. Milton, I. L. Solovtsov, O. P. Solovtsova, Phys. Lett. **B439**, 421 (1998); R. S. Pasechnik, D. V. Shirkov, O. V. Teryaev Phys. Rev. **D78**, 071902 (2008); R. S. Pasechnik *et al.*, Phys. Rev. **D81**, 016010 (2010).  
[19] M. Amarian *et al.*, Phys. Rev. Lett. **92**, 022301 (2004).  
[20] M. Lacombe *et al.*, Phys. Rev. **C 21**, 861 (1980); R. Machleidt, K. Holinde, C. Elster, Phys. Rept. **149**, 1 (1987); M.J. Zuilhof, J.A. Tjon, Phys. Rev. **C 22**, 2369 (1980); K. Kotthoff, R. Machleidt, D. Schutte, Nucl. Phys. **A 264**, 484 (1976); B. Desplanques Phys. Lett. **B 203**, 200 (1988).  
[21] M. E. Christy and P. E. Bosted, Phys. Rev. **C 81** C 055213 (2010).  
[22] O. Filoti, Doctoral dissertation, University of New Hampshire (2007).  
[23] S. Wandzura and F. Wilczek, Phys. Lett. **B 72**, 195 (1977).  
[24] J. Soffer, Phys. Rev. Lett. **74** 1292 (1995).  
[25] S. D. Bass, M. M. Brisudova, Eur. Phys. J. A **4**, 251 (1999).  
[26] V. D. Burkert and B. L. Ioffe, Phys. Lett. **B 296**, 223 (1992); J. Exp. Theor. Phys. **78**, 619 (1994).  
[27] J. Soffer and O. V. Teryaev, Phys. Lett. **B 545**, 323 (2002), Phys. Rev. **D 70**, 116004 (2004).  
[28] R. Pasechnik, J. Soffer and O. Teryaev, Phys. Rev. **D 82**, 076007 (2010).  
[29] E. V. Shuryak and A. I. Vainshtein, Nucl. Phys. **B 201**, 141 (1982); X. Ji and P. Unrau, Phys. Lett. **B 333**, 228 (1994), H. Kawamura *et al.*, Mod. Phys. Lett. **A 12** 135 (1997).  
[30] J. Bluemlein and A. Tkabladze, Nucl. Phys. **B 553** 427 (1999).  
[31] X. Ji, Phys. Lett. **B 309** 187 (1993), X. Ji and W. Melnitchouk, Phys. Rev. **D 56** 1 (1997).  
[32] J. Arrington, W. Melnitchouk and J. A. Tjon, Phys. Rev. **C 76** 035205 (2007).  
[33] P. Mergell, U.-G. Meissner, D. Drechsel. Nucl. Phys. **A**

- 596** 367 (1996).
- [34] J. Bluemlein and H. Boettcher, Nucl. Phys. **B 636**, 225 (2002).
- [35] X. Zheng, *et al.* Phys. Rev. **C70** 065207 (2004).
- [36] P. Solvignon *et al.*, in submission (arXiv:1304.4497).
- [37] M. Posik, *et al.* In submission (arXiv:1404.4003).
- [38] M. Goekeler, Phys. Rev. **D 63**, 074506 (2001).
- [39] A Deur, JLab report <http://tnweb.jlab.org/tn/2008/08-001.pdf>
- [40] CLAS12 Experiment E-12-06-109, S. Kuhn *et al.*, [www.jlab.org/exp\\_prog/proposals/06/PR12-06-109.pdf](http://www.jlab.org/exp_prog/proposals/06/PR12-06-109.pdf)
- [41] E. Stein *et al.*, Phys. Lett. **B 353**, 107 (1995).
- [42] I. I. Balitsky, V. M Braun and A.V. Kolesnichenko, Phys. Lett. **B 242**, 245 (1990); Erratum-*ibid* **B 318**, 648 (1993).
- [43] N.Y. Lee, K. Goetze and C. Weiss, Phys. Rev. **D 65**, 054008 (2002).
- [44] A. V. Sidorov and C. Weiss, Phys. Rev. **D 73**, 074016 (2006).
- [45] E. Leader, A. V. Sidorov, D. B. Stamenov. hep-ph/0612360.
- [46] X. Ji, hep-ph/9510362.
- [47] G. Altarelli, R. D. Ball, S. Forte and G. Ridolfi, Nucl. Phys. **D 496**, 337 (1997).
- [48] C. Amsler *et al.* (Particle Data Group), Phys. Lett. **B 667**, 1 (2008).
- [49] EIC-White Paper, Electron-Ion Collider: Next QCD Frontier. (arXiv:1212.1701)